

<b>Deliverable</b>	<b>D4.2 Report on fracture conductivity measurements within relevant geothermal reservoir rock types under changing load conditions to be used in WP7</b>
<b>Work package</b>	WP4 Micro-Scale
<b>Type</b>	R (document, report)
<b>Dissemination level</b>	PU (public)
<b>Due date</b>	February 28th 2018
<b>Actual submission date</b>	
<b>Lead author (beneficiary)</b>	Christian Kluge (GFZ)
<b>Contributors</b>	Guido Blöcher, Harald Milsch, Chaojie Cheng, David Bruhn
<b>Change History</b>	

## Contents

<b>1 EXECUTIVE SUMMARY</b>	<b>2</b>
<b>2 INTRODUCTION</b>	<b>2</b>
<b>3 SAMPLE MATERIAL &amp; PREPARATION</b>	<b>3</b>
<b>4 METHODS AND EXPERIMENTAL PROCEDURES</b>	<b>3</b>
<b>5 EXPERIMENTAL RESULTS</b>	<b>5</b>
5.1 <i>Permeability of a Single Tensile Fractured &amp; Saw-cut Sample . . . . .</i>	5
5.2 <i>Permeability of a Single Tensile Fracture with Shear Displacement . . . . .</i>	6
5.3 <i>Permeability of a Single Shear Fracture . . . . .</i>	7
<b>6 DISCUSSION</b>	<b>8</b>
<b>7 CONCLUSION</b>	<b>8</b>



# 1 EXECUTIVE SUMMARY

Sustainable energy production is key for today's energy and heat demand and relies on the successful stimulation of low-permeable oil, gas or geothermal reservoirs. Fracture permeability is a substantial topic in recent laboratory and numerical studies. Our aim is to study the sustainability of fracture permeability at varying effective stress with a focus on the fracture mechanism involved.

We aim to further characterize the permeability evolution for different modes, mode I tensile fractures, saw-cut fractures, mode I tensile fractures with shear displacement and mode II shear fractures, in the laboratory, covering all fracture modes commonly observed in EGS. The hydraulic experiments are carried out in a triaxial compression cell. To simulate production and injection procedures in a geothermal reservoir, the effective pressure is varied and permeability is continuously measured.

The permeability development of different fracture types at high effective stresses has been investigated and a general decrease of permeability at already low effective stress was observed in all tests. Shearing does not lead to a sustainable permeability increase for the tested sandstone. Conclusively, any reduction in pore pressure after stimulation will damage the fracture permeability irreversibly.

The results of this study have been originally published as: Kluge, C., Blcher, G., Milsch, H., Hofmann, H., Nicolas, A., Li, Z., Fortin, J. (2017): "Sustainability of fractured rock permeability under varying pressure" - Proceedings, 6th Biot Conference on Poromechanics (Paris, France 2017), pp. 1192-1199.

# 2 INTRODUCTION

The permeability of fractures is key in understanding fluid flow in rocks for a broad range of subsurface applications, e.g. hydraulic fracturing of oil, gas, or geothermal reservoirs, but also in underground constructions, such as nuclear waste repositories. Geothermal reservoir performance of low permeable rocks strongly depends on successful hydraulic stimulation procedures, but it is still not clear how sustainable a stimulation during post-stimulation stage, i.e. injection or production procedures, can be (*Blöcher et al., 2016, e.g.*). A new stimulation technique, Radial Jet Drilling (RJD), is currently investigated within the H2020 SURE\* project, to assess its stimulation performance and potential productivity increase compared to conventional methods, such as hydraulic fracturing. At the laboratory scale, we previously addressed permeability changes of tensile fractures under varying stress conditions: *Hofmann et al. (2016)* investigated the permeability evolution of either aligned or displaced mode I fractures under cyclic variations of confining pressure on pre-fractured granite samples. *Milsch et al. (2016)* analyzed an experiment on a mode I pre-fractured carbonate sample with cyclic confining pressure. The change in permeability of fractures is dependent on many parameters, e.g. rock strength, surface roughness or fractal dimension, pressure and temperature (*Yasuhara and Elsworth, 2008; Raimbay et al., 2017, e.g.*).

In this paper we introduce two innovative methods (asymmetric Brazilian Disk,



Punch-Through Shear test) to generate different types of fractures according to *McClure and Horne (2014)* to measure permeability of single fractured sandstone at high effective pressures. Experiments with tensile and shear fractures, as well as a saw-cut sample are presented and technical challenges are outlined. Permeability evolution as a function of effective pressure and fracture type is examined. Possible reasons for the outcomes are discussed and recommendations for maintaining permeability during the post-stimulation stage are given.

### 3 SAMPLE MATERIAL & PREPARATION

Flechtingen sandstone has been chosen as sample material for various reasons. On one hand, this type of rock is an analogue to the Rotliegend reservoir section in the Groß Schönebeck EGS in the North German basin. The section has been hydraulically stimulated several times due to its low permeability and strong variations in productivity and injectivity (*Blöcher et al., 2016*). On the other hand, the poroelastic behaviour of this rock type has extensively been studied in the past (*Hassanzadegan et al., 2012, e.g.*). Table 1 summarizes the intact rock and fracture properties of each sample ( $\phi$  = porosity,  $k$  = permeability,  $UCS$  = uniaxial compressive strength,  $a$  = optical aperture).

Table 1: *Intact rock & fracture properties of Flechtinger sandstone samples.*

Sample	Fracture type	$\phi$ [%]	$k_{\text{matrix}}$ [mD]	$UCS$ [MPa]	$a$ [ $\mu\text{m}$ ]
<b>Flechtinger S1</b>	saw-cut	12 $\pm$ 1	1.0 $\pm$ 0.2	75.0	165.4 $\pm$ 112.4
<b>Flechtinger S2</b>	tensile	12 $\pm$ 1	1.0 $\pm$ 0.2	75.0	348.7 $\pm$ 127.4
<b>SBT6-BE-01-04</b>	triaxial shear	7.9	0.07	56.7*	-
<b>SBT6-BE-01-13</b>	tensile with shear	7.6	0.07	56.7*	-
<b>SBT6-BE-01-16</b>	tensile	7.7	0.07	56.7*	-

\**Hassanzadegan et al. (2012)*

### 4 METHODS AND EXPERIMENTAL PROCEDURES

A conventional triaxial cell (MTS 815) at the GFZ is used to apply axial load (up to 2000 kN) and confining pressure (up to 140 MPa). A Quizix pump system allows to generate pore pressures of up to 70 MPa and to continuously measure permeability. Temperature is applied via heat belts attached to the outside of the chamber and measured by thermocouples in the cell. For one experiment, a Sanchez triaxial apparatus at the École Normale Supérieure (ENS) in Paris was used. The device applies up to 850 kN axial load and up to 100 MPa confining and pore pressure. All experiments were performed at a temperature of 30°C, except the one at ENS (controlled at 21°C). A differential fluid pressure sensor measures the difference in up- and downstream pressure. At the Sanchez triaxial press, the difference in upstream and downstream pressure of the pumps is regarded as differential fluid pressure. The cylindrical samples have the dimensions of 50x100 mm (GFZ) and 40x80 mm (ENS), respectively. Sample permeability ( $k$ ) is calculated using Darcy's



law and hydraulic fracture aperture ( $a_h$ ) via the cubic law assumption. The hydraulic aperture is  $a_h = \sqrt[3]{6\pi kr}$ , where  $r$  is the sample radius (*Hofmann et al., 2016*). With the assumption that the UCS ( $P_{ucs}$ ) controls the contact area of the fracture faces, the change in contact area can be calculated using a force balance approach (*Milsch et al., 2016*):  $A_c = (P_{eff}/P_{ucs})A_s$ , where  $A_c$  is the true contact area and  $A_s$  the apparent contact area ( $50 \text{ cm}^2$ ).

**Tensile fractured & saw-cut rock without shear displacement.** A cylindrical sample covered in a heat-shrink tube was loaded diametrically using the Brazilian Disk (BD) test creating a single tensile fracture. After installation in a triaxial cell, axial load and confining pressure was applied (fig. 1a). While varying pore pressure (SBT6-BE-01-16) or varying confining pressure (Flechtinger S1/S2), the rock permeability was measured continuously using a differential pressure sensor. Saw-cut samples can be used to simulate fractures with a given roughness and aperture. Two samples were cut in half so that one remaining half of each sample has a radius of 2.5 cm, giving the required sample diameter of 5 cm.

**Tensile fractured rock with shear displacement.** A cylindrical sample was split into two halves using the BD setup. Hemi-cycle shaped spacers made of steel and teflon with perforations allowing fluid transmission were placed at the top and bottom of the sample (fig. 1b). They were positioned such that steel and teflon are opposite to each other to create asymmetric loading conditions due to their different elastic moduli  $E_{teflon} \sim 0.5 \text{ GPa}$  and  $E_{steel} \sim 180 \text{ GPa}$ . After varying the effective pressure, a displacement controlled axial loading ramp was started. This results in asymmetric loading conditions, creating a shear displacement along the pre-existing fracture.

**Triaxial shear test.** A shear fracture was created at increased pore pressure by decreasing the effective stress acting on the grain contacts under differential loading conditions (fig. 1c). When the sample started yielding, axial loading was stopped and a high fluid pressure was applied on one side of the sample causing the rock to fail. After that, at constant ambient stresses, pore pressure was varied in cycles to measure the post-failure permeability of the fractured sample at different effective stresses.

**Punch-Through Shear test.** To investigate the permeability evolution in shear fractures, the PTS can be adapted to allow fracture parallel fluid flow within the sample (fig. 1d). The setup consists of an upper and lower loading stamp that is designed to create a circular shear fracture by pushing down the inner cylinder of a notched cylindrical rock sample. The 1 mm wide and 10 mm deep notch causes a stress concentration at the tip to better control fracture initiation. The displacement will create a shear stress at the notch tip leading to shear fracture initiation and propagation towards the lower notch of the sample.



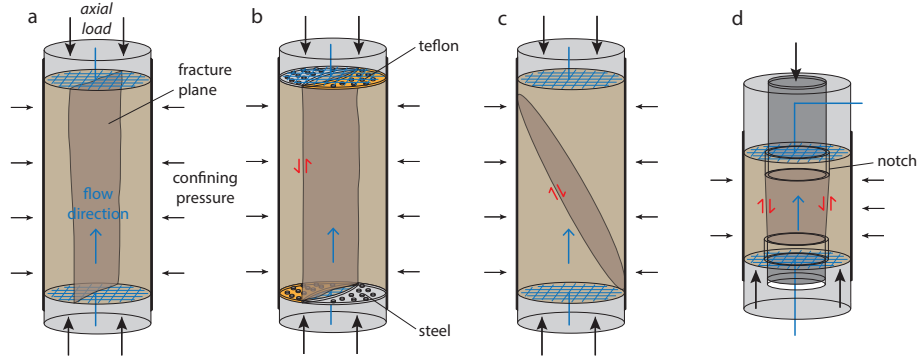


Figure 1: *Experimental setups and fracture types: a) tensile fractures, saw-cut samples; b) tensile fractures with shear displacement; c) triaxial shear fracture and d) pure shear fracture.*

## 5 EXPERIMENTAL RESULTS

### 5.1 Permeability of a Single Tensile Fractured & Saw-cut Sample

Permeability of a tensile fracture was measured on two samples of Flechtinger sandstone. In one experiment (Flechtinger S2), the confining pressure was increased to 40 MPa and then decreased to 2 MPa at constant pore pressure (0.1-0.7 MPa). The permeability reduced when effective pressure increased, but the change in permeability became smaller at higher pressure (fig. 2a). When effective pressure was again decreased by decreasing confining pressure, the permeability increased, but remained at a lower value compared to similar effective pressure levels before. In another experiment (SBT6-BE-01-16), pore pressure was varied at constant confining pressure (20 MPa) showing an irreversible decrease in permeability once the pore pressure was reduced (fig. 2b). For the saw-cut sample (S1) with higher initial permeability ( $\sim 75$  mD), the confining pressure was increased at constant pore pressure. With increasing effective pressure the permeability was reduced by almost one order of magnitude and remained in the following cycles at a residual permeability of  $\sim 1$  to 4 mD (fig. 2c). The apertures of the fracture and saw-cut were measured optically using a microscope (fig. 3). The average initial aperture was  $165.4 \mu\text{m}$  for the tensile fracture and  $348.7 \mu\text{m}$  for the saw-cut. After the experiment, aperture was reduced to  $32.3 \pm 11.8$  for the fractured sample. Hydraulic aperture reduced from  $6.78$  to  $3.84 \mu\text{m}$  for sample S2 and from  $32.8$  and  $14.7 \mu\text{m}$  for sample S1 at 2 and 40 MPa effective pressure, respectively. Hydraulic aperture for sample SBT6-BE-01-16 is  $3.28$  and  $1.52 \mu\text{m}$  at 2 and 15 MPa effective pressure, respectively. The increase of true contact area ( $\Delta A_c$ ) is  $12.0 \text{ cm}^2$  when effective pressure is increased from 1 to 19 MPa, and  $25.3 \text{ cm}^2$  when increased from 1 to 39 MPa (for UCS of 75 MPa).

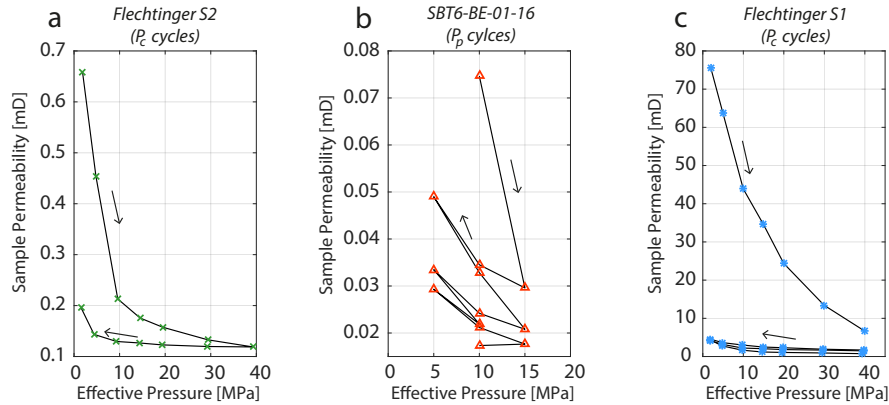


Figure 2: Permeability evolution of tensile fractured (a,b) and saw-cut (c) samples.



Figure 3: Optical aperture of tensile fracture before and after testing (a,b); and the saw-cut (c).

## 5.2 Permeability of a Single Tensile Fracture with Shear Displacement

Initially, hydrostatic and pore pressure was increased and varied stepwise (sample SBT6-BE-01-13). Effective pressure increase leads to a reduction of permeability, but a following decrease cannot recover the previous permeability. In the respective pressure cycles, permeability decreased from 44 mD to 3 mD (fig. 4, left). At an effective pressure of 10 MPa ( $P_c=20$  MPa,  $P_p=10$  MPa) the sample was axially loaded with a displacement rate of 0.0001 mm/sec. The axial displacement was increased by 1.5 mm. At around 1 mm, the sample started yielding with a following drop in the load curve (fig. 4, right). At this point, the permeability slightly increased. Continuing the axial displacement ramp, two significant stress drops were observed. Both were associated with a rapid but short increase in permeability followed by an instant decrease in permeability. A following increase in pore pressure did not lead to another slip event. Instead, the axial load decreased at a constant rate (creep). During unloading, the sample permeability decreased further until almost matrix permeability was reached (fig. 4, left). A small increase is observed when effective pressure reaches 2 MPa. Unintended, new sets of shear fractures formed (fig. 5). They initiated at the top of the sample close to the border of the steel spacer, but not at the pre-existing tensile fracture. Only a very little displacement (up to  $\sim 0.2$  mm) could be observed along the tensile fracture, but some relative displacement was related to the newly created shear fractures.

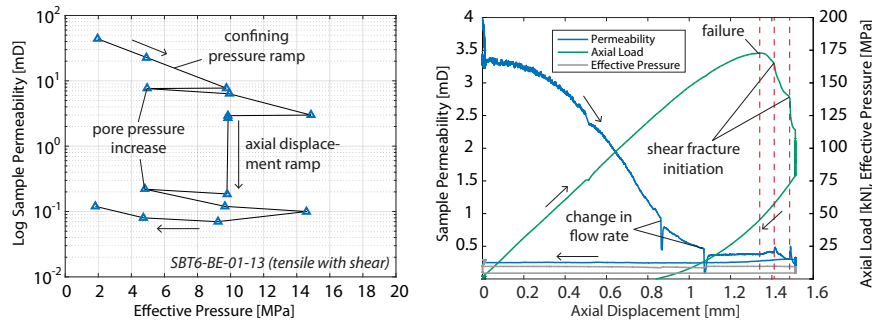


Figure 4: *Permeability at varying effective pressures (left) and with axial displacement (right).*

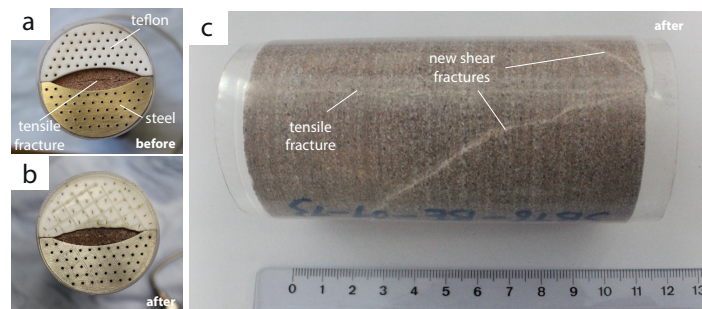


Figure 5: *Spacers and sample before (a) and after testing (b,c), showing new fractures.*

## 5.3 Permeability of a Single Shear Fracture

The triaxial shear experiment was performed using the testing device at ENS (SBT6-BE-01-04). The sample failed under triaxial loading conditions at elevated pore pressure and constant ambient stresses in shear mode (fig. 6, left). Flow was not parallel to the fracture since the fracture did not cut through the end faces of the sample, and an inclined shear fracture could be observed post-mortem (at 63.5°). After failure, the pore pressure was varied. The permeability was then measured over the entire length of the sample at varying effective pressures ranging from around 5 to 20 MPa. Permeability decreased each time when effective pressure is increased (fig. 6, right).

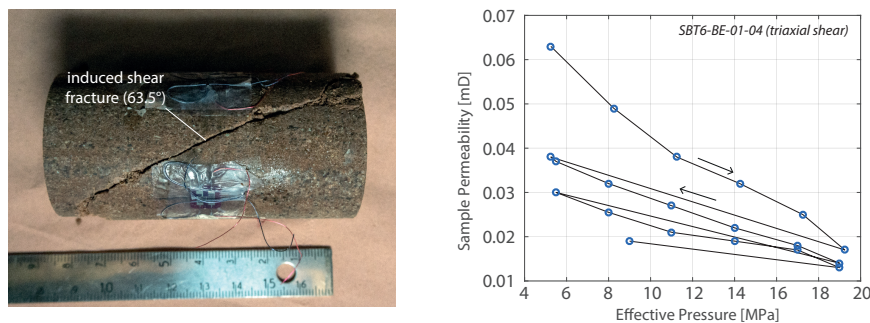


Figure 6: *Permeability evolution of a shear fracture at varying effective pressure.*

## 6 DISCUSSION

Overall, initial rock permeability was damaged in both tensile fracture tests and the shear test when comparing the permeability after testing the fractured rock with the intact rock permeability. Only the saw-cut and the tensile fracture with shear displacement retained a higher permeability compared to the intact rock permeability. This behaviour, however, is dependent on the initial fracture aperture generated in the Brazilian Disk test. For tensile fractures, the reduction in permeability can be described as a result of fracture closing and failure of asperities under external pressure and therefore a reduction in aperture. Here, fracture aperture and contact area are linked such that the contact-area ratio is approximated by the Hertzian contact theory (*Yasuhara and Elsworth, 2008*). Most of the deformation already occurs at low normal stresses. Tensile fractures are less sustainable because of the interlocking of perfectly matching, non-displaced asperities compared to the two mismatching surfaces of the saw-cut sample. At elevated effective pressure fracture permeability evolution was observed as time-dependent creep-like closure, which was also described by *Milsch et al. (2016)*. Increasing the axial displacement under asymmetrical loading conditions on a pre-fractured sample yielded a small increase in fracture offset. This results in a slow decrease in permeability, possibly because of particles and asperities being crushed. The newly generated fractures initiated at the top of the sample, towards the mantle area, but not at the pre-existing tensile fracture itself. A possible explanation is that frictional shear stress oversteps the yield strength of the intact sample at elevated confining pressures (*Milsch and Scholz, 2005*). Although at the point of shear fracture initiation, the permeability increases for a short moment, it decreases immediately after that. The shear fracture is probably mylonized such that grains in the fracture zone are crushed and rotated, forming an impermeable shear band. The advantage of testing in a triaxial cell are the additional differential stresses applied, while conventional shear-box setups only allow a normal stress. The question remains, whether shear fractures are in contact during shearing (abrasion) while hydraulic stimulation in reservoirs or whether the fracture faces are separated by a distance. For the triaxial shear experiment with a fluid induced shear fracture permeability remained at almost matrix permeability. At large variations of the measured fractured rock permeability and matrix permeability, the measured value can be attributed to fracture flow. Compaction of the matrix during the pressure cycles or permeability measurements can be neglected, since ambient pressures were either constant or below the integrity limit of the sample (*Heiland and Raab, 2001*), except in the experiment with a tensile fracture with axial displacement.

## 7 CONCLUSION

Different experimental approaches have been used to determine the permeability evolution of fractured sandstone rock with focus on the different fracture modes (tensile, tensile with shear, shear) under varying effective pressures. The following conclusions can be drawn: (a) tensile fractures will increase the permeability only during the initial stage, since already low normal stresses will reduce the permeability; (b) permeability of tensile



and shear fractured (non-parallel flow) samples are lower than the initial intact rock permeability, whereas saw-cut samples and tensile fractures with shear displacement retain an improved permeability after the pressure cycles; (d) a modified PTS test was suggested to allow measurements at fracture parallel flow conditions and will be tested soon. For post-stimulation strategies, a pore pressure decrease after stimulation might result in an irreversible damage to the permeability of the fractures. Additional experiments at varying temperatures with different rock types are in the planning and numerical simulations will be set up to better understand fluid flow behaviour within a fracture-matrix system.

## References

- Blöcher, G., Reinsch, T., Henninges, J., Milsch, H., Regenspurg, S., Kummerow, J., Francke, H., Kranz, S., Saadat, A., Zimmermann, G., and Huenges, E. (2016). Hydraulic history and current state of the deep geothermal reservoir groß schönebeck. *Geothermics*, 63:27–43.
- Hassanzadegan, A., Blöcher, G., Zimmermann, G., and Milsch, H. (2012). Thermoporoe-  
lastic properties of flechtinger sandstone. *International Journal of Rock Mechanics and Mining Sciences*, 49:94–104.
- Heiland, J. and Raab, S. (2001). Experimental investigation of the influence of differential stress on permeability of a lower permian (rotliegend) sandstone deformed in the brittle deformation field. *Physics and Chemistry of the Earth, Part A: Solid Earth and Geodesy*, 26(1-2):33–38.
- Hofmann, H., Blöcher, G., Milsch, H., Babadagli, T., and Zimmermann, G. (2016). Transmissivity of aligned and displaced tensile fractures in granitic rocks during cyclic loading. *International Journal of Rock Mechanics and Mining Sciences*, 87:69–84.
- McClure, M. W. and Horne, R. N. (2014). An investigation of stimulation mechanisms in enhanced geothermal systems. *International Journal of Rock Mechanics and Mining Sciences*, 72:242–260.
- Milsch, H., Hofmann, H., and Blöcher, G. (2016). An experimental and numerical evaluation of continuous fracture permeability measurements during effective pressure cycle. *International Journal of Rock Mechanics and Mining Sciences*, 89:109–115.
- Milsch, H. and Scholz, C. H. (2005). Dehydration-induced weakening and fault slip in gypsum: Implications for the faulting process at intermediate depth in subduction zones. *Journal of Geophysical Research: Solid Earth*, 110(B4).
- Raimbay, A., Babadagli, T., Kuru, E., and Develi, K. (2017). Fractal analysis of single-phase water and polymer solution flow at high rates in open and horizontally displaced rough fractures. *International Journal of Rock Mechanics and Mining Sciences*, 92:54–71.



Version 2/26/2018	Project SURE - Grant-Number 654662	page 10 / 10
-------------------	------------------------------------	--------------

Yasuhara, H. and Elsworth, D. (2008). Compaction of a rock fracture moderated by competing roles of stress corrosion and pressure solution. *Pure and Applied Geophysics*, 165(7):1289–1306.

